Submitted to

XXII International Symposium on Lepton-Photon Interactions at High Energy, June 30^{th}, 2005, Uppsala

Abstract: **408**

Session : **Flavor physics** and **QCD and hadron structure**

www-h1.desy.de/h1/www/publications/conf/conf_list.html

The Structure of Charm Jets in Deep-Inelastic Scattering

H1 Collaboration

Abstract

The structure of charm jets in deep-inelastic scattering is studied with the H1 detector at HERA using an integrated luminosity of 50 pb^{-1}. The event samples are in the phase space region $2 \leq Q^2 \leq 100$ GeV^2 and $0.05 \leq y \leq 0.7$. The charm events are tagged by a D^*-meson required to have a transverse momentum $p_{\mathrm{t},D^*} > 1.5$ GeV and a pseudorapidity $|\eta_{D^*}| < 1.5$. Furthermore, the events are required to have at least one jet containing the D^*-meson ($D^*\mathrm{Jet}$). If there is a second jet ($Other\mathrm{Jet}$) in the event, it must have, like the $D^*\mathrm{Jet}$, $p_{\mathrm{t,jet}} > 1.5$ GeV and $|\eta_{\mathrm{jet}}| < 1.5$. The structure of the $D^*\mathrm{Jet}$ and the $Other\mathrm{Jet}$ is investigated by measuring jet shapes variables and subjet multiplicities, as well as the angular distribution of a subjet of the $D^*\mathrm{Jet}$ and the $Other\mathrm{Jet}$ with respect to the direction of its respective jet. This novel angular distribution is defined to give a correlation with a corresponding gluon at the parton level and is motivated by the suppression of soft gluon radiation from heavy quarks, as expected from QCD. In all distributions differences between the $D^*\mathrm{Jet}$ and the $Other\mathrm{Jet}$ are observed. The data are found to be well described by the QCD model for charm production as implemented in RAPGAP 2.8 and JETSET 7.4.

1 Introduction

The internal structure of the light quark jets has been studied extensively both from a theoretical and experimental point of view. The experimental data [1] [2] from ep collisions at HERA are in good agreement with the predictions of QCD based models. Measurements [3] of subjet multiplicities and jet shapes have been used to extract values of the strong coupling, leading to results consistent with the world average and having competitive uncertainty.

Jets initiated by heavy quarks are expected to be different from those initiated by light quarks. In the case of heavy quarks, the phase space available for gluon emissions is reduced due to the heavy quark mass [4] [5]. Also the fragmentation of heavy quarks is much harder than for light flavors.

In this analysis we investigate the structure of charm jets identified via the reconstruction of the D^*-meson. The jet shape observables, $< \psi(r/R) >$ and $< \rho(r/R) >$, and mean subjet multiplicities are measured. In addition, the angular distribution of a specific subjet of the charm jet with respect to the charm jet and its dependence on the charm jet energy is studied. This distribution might be expected to be sensitive to the suppression of soft gluons from heavy quarks close to their direction of flight. For such gluons the differential cross section can be approximated by [5]:

$$\frac{d\sigma_{Q \to Q+g}}{d\alpha} \approx K \frac{\alpha^3}{(\alpha_0^2 + \alpha^2)^2} \ , \tag{1}$$

where

$$\alpha_0 = M_Q / E_Q \ , \tag{2}$$

with M_Q being the mass of the heavy quark and E_Q its energy. The angle between the radiated gluon and the primary heavy quark momentum is denoted by α. It follows from eq. 1 that in the region of small α the emission of soft gluons is suppressed, and therefore this region is called the "dead cone". It is characterized by an opening angle α_0 which depends on the mass and energy of the heavy quark. In section 2 an attempt is made to define an experimentally accessible angle which should approximate the parton level angle α.

Indirect evidence for the presence of the dead cone, based on comparing multiplicities in light-quark and heavy-quark jets has been reported by the DELPHI collaboration [6].

At HERA the charm quarks are produced mainly via the boson-gluon fusion process [7]. Most of the charm quarks are produced in pairs and, in contrast to most e^+e^- experiments, close to the kinematic threshold. This allows to study the effect of the charm mass on jet structure at low jet momenta, in a region of phase space, where these effects are expected to be measurable with H1 detector.

2 Experimental Method

Deep-inelastic scattering (DIS) events with charm are tagged by reconstructing a D^*-meson[1] using the channel $D^{*+} \to D^0 \pi_s^+ \to K^- \pi^+ \pi_s^+$. As soon as a D^* is found in an event, it is treated as one particle and its decay products are discarded.

[1] D^* refers to both D^{*+} and D^{*-} states.

Jets are found using the inclusive $k_{\rm t}$ cluster algorithm, applied in the laboratory frame. The input to the jet-finding algorithm are hadronic objects [12], created on the basis of combined information from calorimetric energy clusters and tracks. The particle tracks reconstructing the D^*-meson are discarded. The events with at least one jet containing a D^*-meson and having $p_{\rm t,jet} > 1.5$ GeV are accepted. The properties of this jet, the $D^*{\rm Jet}$, and of the largest $p_{\rm t}$ jet which does not contain the reconstructed D^*-meson, the $Other{\rm Jet}$, if observed within fiducial limits, are studied using the jet shape observables.

To find subjets at least two hadronic objects in addition to the D^* are required, the $k_{\rm t}$ cluster algorithm is re-run on the hadronic objects belonging to the $D^*{\rm Jet}$ and $Other{\rm Jet}$, varying the resolution parameter $y_{\rm cut}$ until two subjets are found.

More details on the event and particle selection can be found in section 4.

The observables used to study the energy flow inside a jet are the jet shape variables defined as:

$$< \psi(r/R) >= \frac{1}{N_{\rm jets}} \sum_{\rm jets} \frac{E_{\rm t,jet}(r)}{E_{\rm t,jet}(r=R)} \ , \tag{3}$$

where $E_{\rm t,jet}(r)$ is the total transverse energy of particles inside a cone with size $r = \sqrt{\Delta\phi^2 + \Delta\eta^2}$ around the jet axis[2], $R = 1$, and

$$< \rho(r/R) >= \frac{d\psi}{dr} = \frac{1}{N_{\rm jets}} \sum_{\rm jets} \frac{E_{\rm t,jet}(r, r+\Delta r)}{E_{\rm t,jet}(r=R)} \ , \tag{4}$$

where $E_{\rm t,jet}(r, r+\Delta r)$ is total transverse energy of particles between a cone with size r and one with $r + \Delta r$.

The mean subjet multiplicity is defined as the number of subjets inside the jet, found by the inclusive $k_{\rm t}$ jet finder algorithm [10] as a function of the jet resolution parameter $y_{\rm cut}$.

$$< n_{\rm sbj}(y_{\rm cut}) >= \frac{1}{N_{\rm jets}} \sum_{i=1}^{N_{\rm jets}} n^i_{\rm sbj}(y_{\rm cut}) \tag{5}$$

Finally, to approximate the angular distribution of the soft gluons with respect to the jet direction we propose to measure the distribution of the soft "gluon" subjet angle, α, as a function of $E_{D^*{\rm Jet}}$ and $E_{Other{\rm Jet}}$. The subjets are found by re-running the jet finder algorithm on particles inside the $D^*{\rm Jet}$ and the $Other{\rm Jet}$ with a decreasing resolution parameter $y_{\rm cut}$ until two subjets are found (see Fig. 1 and 2). The "gluon" subjet angle α is defined as the angle between the direction of the $D^*{\rm Jet}$ and the direction of the subjet not containing the D^*-meson. For the $Other{\rm Jet}$ is is defined as the angle between the direction of the $Other{\rm Jet}$ and the direction of the less energetic subjet.

According to eq. 1 one expects the angular distribution to shift to smaller angles with increasing jet energy. It turns out that the experimental angular distributions can be fit to the QCD prediction, in the small angle region, where it should be valid. This allows to determine values

[2]Here and later in the article η denotes the pseudorapidity of a particle: $\eta = -\ln\left[\tan\left(\frac{\theta}{2}\right)\right]$.

for α_0 for different jet energies. From eq. 2 one expects that the distribution $\alpha_0\ E_{\rm jet}$ is independent of the jet energy, i. e. a constant of size M_Q. In Fig. 3 the parton model predictions of a QCD model[3], which includes soft gluon suppression, are shown. Two different "charm" masses $(1.4\ (\mathrm{default}), 1.8$ GeV) were used. One can see the expected effect. For the light quarks, in contrast to charm, the level for the "mass" is at about 1 GeV. This is due to the fact that in the QCD model partons with invariant mass Q_0 (1 GeV) are assumed not to radiate any further. When the Q_0 is reduced to e.g. $2.2\Lambda_{QCD}$ ($\Lambda_{QCD} = 0.29$ GeV) this "mass" is seen to drop as expected.

In Fig. 4 the correlation in η and ϕ between the $D^*\mathrm{Jet}$ ($Other\mathrm{Jet}$) and the corresponding charm quark is shown for two different jet energy bins. While for the $D^*\mathrm{Jet}$ the correlation is excellent in all energy bins, for the $Other\mathrm{Jet}$ it degrades at low energies, i. e. the corresponding charm jet is not so well reconstructed or is even not found at all. It is therefore expected that the eq. 2 will be difficult to be verified experimentally in case of the $Other\mathrm{Jet}$, for energies below about 5 GeV.

The analysis has been carried out in the laboratory frame. In order to check that the corresponding results are not due to this particular frame, the distributions of the angle α was also determined in a frame, where the respective jet is always normal to the γp direction. This frame is referred to as the $n\gamma p$- frame[4].

3 Detector and Data Sample

The data presented here were collected with the H1 detector during the running periods of 1999 and 2000. In that period HERA operated with 27.6 GeV positrons and 920 GeV protons, colliding them at a center-of-mass energy of $\sqrt{s} \sim 320$ GeV. The data, after applying quality requirements on the detector components, amount to an integrated luminosity of 50 pb^{-1}. A detailed description of the H1 detector is given in [8] and [9], and the components most relevant for this analysis are discussed in [7].

4 Data Selection

The analysis is performed in DIS, with the scattered positron detected in the backward calorimeter (SpaCal). In order to ensure high acceptance for the entire kinematic region, the square of the four momentum transfer is restricted to $2 \le Q^2 \le 100$ GeV^2 and the inelasticity to $0.05 \le y \le 0.7$. The energy of the scattered positron is required to be larger than 8 GeV. The positron identification is verified by checking for track segments in the backward drift chamber. In order to suppress background, cuts on the position of the event vertex ($|z_{\rm vtx}| < 35$ cm) and on the quantity $E - p_z$, summed over all hadronic particles and the scattered positron,

[3] RAPGAP 2.8/ JETSET 7.4 is used. Only the direct process $\gamma g \to c\bar{c}$ is generated.

[4] The $n\gamma p$- frame [11] is defined by boosting the respective jet and its subjets first to the γp- frame and then in the $-p_{\rm z,jet}$ direction.

$(40 < E - p_z < 75$ GeV) are applied. The kinematic variables Q^2 and y are calculated from the energy E'_e and the polar angle θ_e of the scattered positron[5].

The charm events charm are tagged by reconstructing the D^*-meson using the channel $D^{*+} \to D^0\pi_s^+ \to K^-\pi^+\pi_s^+$. The range of transverse momentum and pseudorapidity of the D^*-meson is restricted to $p_{t,D^*} > 1.5$ GeV and $|\eta_{D^*}| < 1.5$. These cuts are applied in order to ensure that the events lie in a region of the detector where the acceptance is high and very well understood.

The kinematic cuts, applied to the individual charged particle tracks, are: $p_{t,\pi_s} > 0.12$ GeV, $p_{t,K,\pi} > 0.25$ GeV, $|\eta_{K,\pi,\pi_s}| < 1.5$ and $p_{t,K} + p_{t,\pi} > 2$ GeV. The D^0 mass window cut is $|m_{K\pi} - m_{D^0}| < 0.07$ GeV. The D^* signal is identified using the well known mass difference $\Delta m = m_{K\pi\pi_s} - m_{K\pi}$. The background is subtracted using the wrong-charge (WrCh)[6] events in the Δm range $0.143 < \Delta m < 0.148$ GeV. The normalization of WrCh background is determined from a simultaneous fit to both the right-charge (RiCh) and WrCh Δm distributions.

The Δm spectra for the sample fulfilling the D^*Jet and subjets requirements are presented in Fig. 5. The number of D^*-mesons is 1584 ± 70.

All measured observables are shown at the detector level[7] and are compared with the predictions of the RAPGAP 2.8 MC model [13], which were used as input to the detailed H1 detector simulation and reconstruction package.

Several sources of systematic errors have been investigated. The energy of the scattered positron has been varied by $\pm 1\%$, and the polar angle of the scattered positron has been changed by ± 2 mrad. The systematic error caused by the uncertainty of the hadronic energy scale has been estimated by varying the energy of each hadronic object by $\pm 4\%$. The effect of the jet radius on the reconstruction of the "correct" charm quark energy, the uncertainty due to the D^*-signal extraction procedure and the error on the α_0 values by fitting the α distributions have been studied. The individual systematic errors have been added in quadrature.

5 Results

For this sample the following "control" distributions are shown in Fig. 6: the energy spectrum and pseudorapidity distribution of the D^*Jet and the $Other$Jet. They are in reasonable agreement with the QCD model prediction, provided by RAPGAP 2.8. Also the azimuthal opening angle between the D^*Jet and the $Other$Jet shows the expected back-to-back topology in the $\gamma^* p$-frame as it can be seen in Fig. 7.

The jet shape variables $< \psi >$ and $< \rho >$ as a function of r/R, and the number of subjets $< n_{\rm sbj} >$ as a function of the resolution parameter $y_{\rm cut}$ are presented in Fig. 8. The significant differences observed between the distributions of the D^*Jet and the $Other$Jet are largely due to the requirement of a reconstructed D^*-meson in the former. The data are compared with QCD model predictions indicating reasonable agreement.

[5] $Q^2 = 4E_e E'_e \cos^2\left(\frac{\theta_e}{2}\right)$; $y = 1 - \frac{E'_e}{E_e}\sin^2\left(\frac{\theta_e}{2}\right)$.

[6] WrCh: $D^{*+} \to K^+\pi^+\pi_s^-$ and charge conjugate.

[7] The α distributions have been calculated also at the level of the partons and hadrons in the MC.

Fig. 9 gives the distribution of the "gluon" subjet angle α for the $D^*\mathrm{Jet}$ in data and Monte Carlo, after full detector simulation and reconstruction, for two representative bins in jet energy. The data indicate the same behaviour as the model. The angular distribution shifts towards smaller angles with increasing jet energy for both data and QCD model. The solid line shows the result of a fit using the function $f(\alpha) = A\alpha^3/(\alpha_0^2 + \alpha^2)^2$, motivated by the QCD prediction of eq. 1. Two parameters, a normalization factor and the size of α_0, are left free in the fit. The fit describes data and model reasonably well.

In Fig. 10 the parameter α_0 multiplied by the E_{jet} for the $D^*\mathrm{Jet}$ and the $Other\mathrm{Jet}$ is shown as a function of the jet energy. It is reasonably well described by the QCD model prediction. A similar good agreement is found when boosting the jets from the laboratory into the $n\gamma p$-frame, defined in sect. 2.

It may be tempting to interpret the observed flatness of the distribution and the observed value as being due to the dead cone effect for charm quarks. However, this interpretation is not supported by the distributions shown in Fig. 11. Here, in addition to the $D^*\mathrm{Jet}$ and $Other\mathrm{Jet}$ data from the previous Fig. 10, distributions labeled "fake" $D^*\mathrm{Jet}$: WrCh and "fake" $Other\mathrm{Jet}$: WrCh are presented, which are obtained by finding a "fake" $D^*\mathrm{Jet}$, where the wrong charge particle combinations have been found to lie in the D^0 and D^* signal regions.

The additional distributions labeled 2Jet instead of WrCh in Fig. 11 are obtained by performing a right charge selection for the D^*, as for the $D^*\mathrm{Jet}$ and $Other\mathrm{Jet}$ sample, however on a flavor-unbiased dijet sample (i. e. no online reconstructed D^*-meson requirement as for the charm selection). Also no track requirements on transverse momenta and dE/dx, designed to enhance the charm signal with respect to the background, were imposed and no background subtraction was done.

The distributions look somewhat different from the ones from charm jets but, 'agree' within the current errors[8]. Besides an increase in statistics further studies are needed to clarify the origin of these differences. Thus the present results do not allow yet any conclusion concerning the dead cone effect.

6 Conclusion

The internal structure of charm jets has been investigated and compared to a QCD based Monte Carlo model (RAPGAP 2.8 / JETSET 7.4). All observables, the jet shape variables ψ and ρ, the subjet multiplicity, and the distribution of $\alpha_0 E_{\mathrm{jet}}$ for the $D^*\mathrm{Jet}$ and the $Other\mathrm{Jet}$ are fairly well described by the model, including the clear differences observed between the distributions for charm jets including a D^*-meson ($D^*\mathrm{Jet}$) and those which do not ($Other\mathrm{Jet}$).

The distribution of $\alpha_0 E_{\mathrm{jet}}$ has been measured in order to investigate the suppression of soft gluon emission from charm quarks at HERA. While it and all other observables are found to be consistent with predictions from a QCD model which, among other effects, also implements this dead cone effect, no clear direct evidence for the latter has been obtained with the present statistics.

[8]The distributions referring to $D^*\mathrm{Jet}$ and $Other\mathrm{Jet}$ indicate statistical and systematic errors, while the distributions referring to 2Jet show only the statistical errors.

References

[1] J. Breitweg *et al.* [ZEUS Collaboration], Eur. Phys. J. C **2** (1998) 61 [hep-ex/9710002]; J. Breitweg *et al.* [ZEUS Collaboration], Eur. Phys. J. C **8** (1999) 367 [hep-ex/9804001].

[2] C. Adloff *et al.* [H1 Collaboration], Nucl. Phys. B **545** (1999) 3 [hep-ex/9901010].

[3] S. Chekanov *et al.* [ZEUS Collaboration], Phys. Lett. B **558** (2003) 41 [hep-ex/0212030]; S. Chekanov [ZEUS Collaboration], Nucl. Phys. B **700** (2004) 3 [hep-ex/0405065].

[4] Y. L. Dokshitzer, V. S. Fadin and V. A. Khoze, Z. Phys. C **18** (1983) 37.

[5] Y. L. Dokshitzer, V. A. Khoze and S. I. Troian, J. Phys. G **17** (1991) 1602.

[6] P. Abreu et al. [DELPHI collaboration], *Phys. Lett.* B**479** (2000) 118.

[7] C. Adloff et al. [H1 Collaboration], Z. Phys. C **72** (1996) 593 [hep-ex/9607012].

[8] I. Abt et al. [H1 collaboration], *Nucl. Instrum. Methods* A**386** (1997) 310.

[9] I. Abt et al. [H1 collaboration], *Nucl. Instrum. Methods* A**386** (1997) 348.

[10] S. D. Ellis and D. E. Soper, Phys. Rev. D **48**, 3160 (1993) [hep-ph/9305266]; S. Catani et al. Nucl. Phys. B **406**, 187 (1993).

[11] W. Ochs, private communication.

[12] M. Peez, B. Portheault, E. Sauvan, H1-IN-(616/2005).

[13] H. Jung, *Comp. Phys. Commun.* **86** (1995)147.

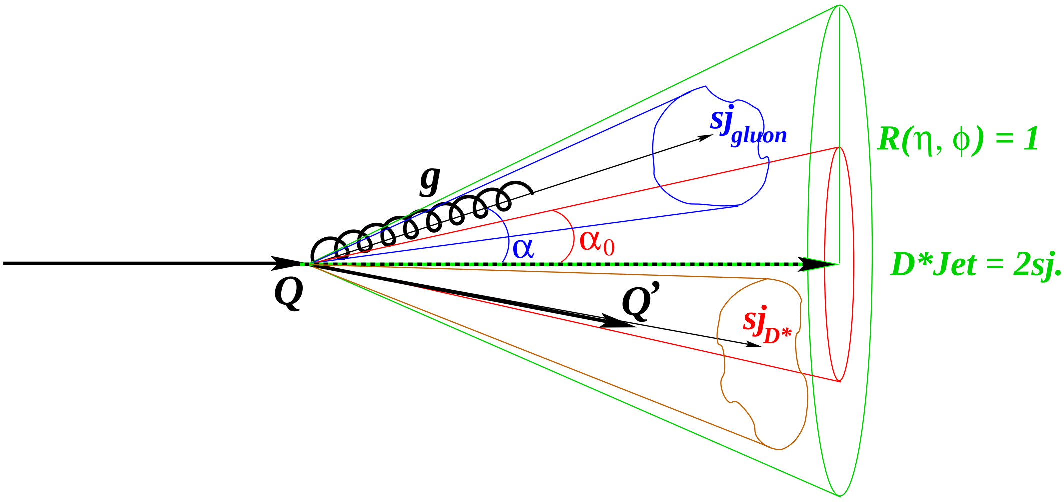

Figure 1: The definition of the "gluon" subjet angle for the D^*Jet
(sj_{gluon} is the one not containing the D^*-meson)
$\alpha = \measuredangle(D^*\text{Jet}, sj_{gluon})$.

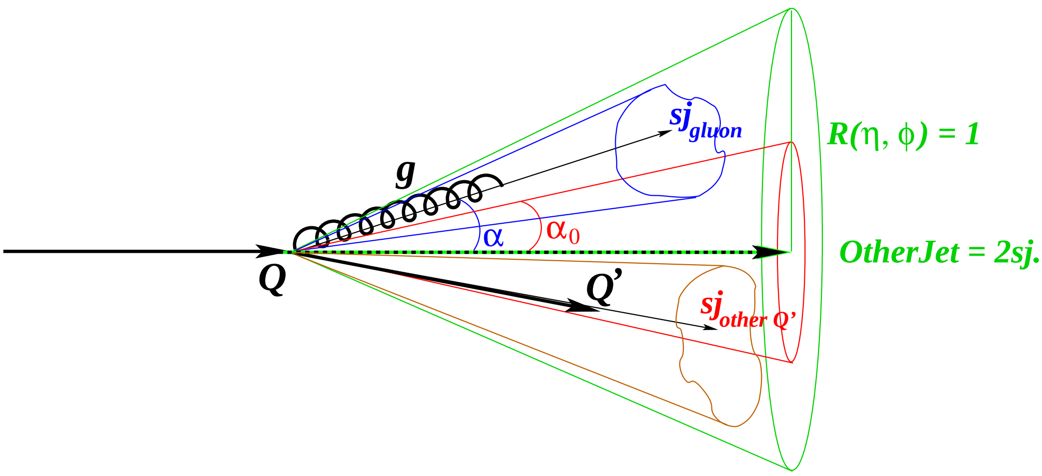

Figure 2: The definition of the "gluon" subjet angle for the $Other$Jet
(sj_{gluon} is the less energetic one of the two subjets)
$\alpha = \measuredangle(Other\text{Jet}, sj_{gluon})$.

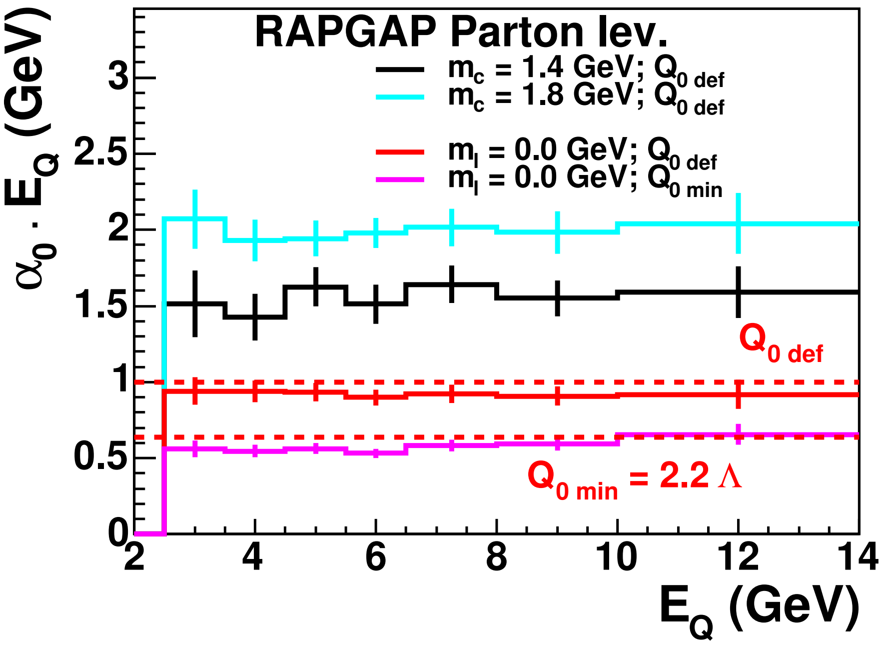

Figure 3: $\alpha_0\ E_Q$ as a function of E_Q at the parton level.
($Q_{0\ def} = 1$ GeV, $Q_{0\ min} = 2.2\Lambda$, $\Lambda = 0.29$ GeV).
The dashed lines show the different values of Q_0.

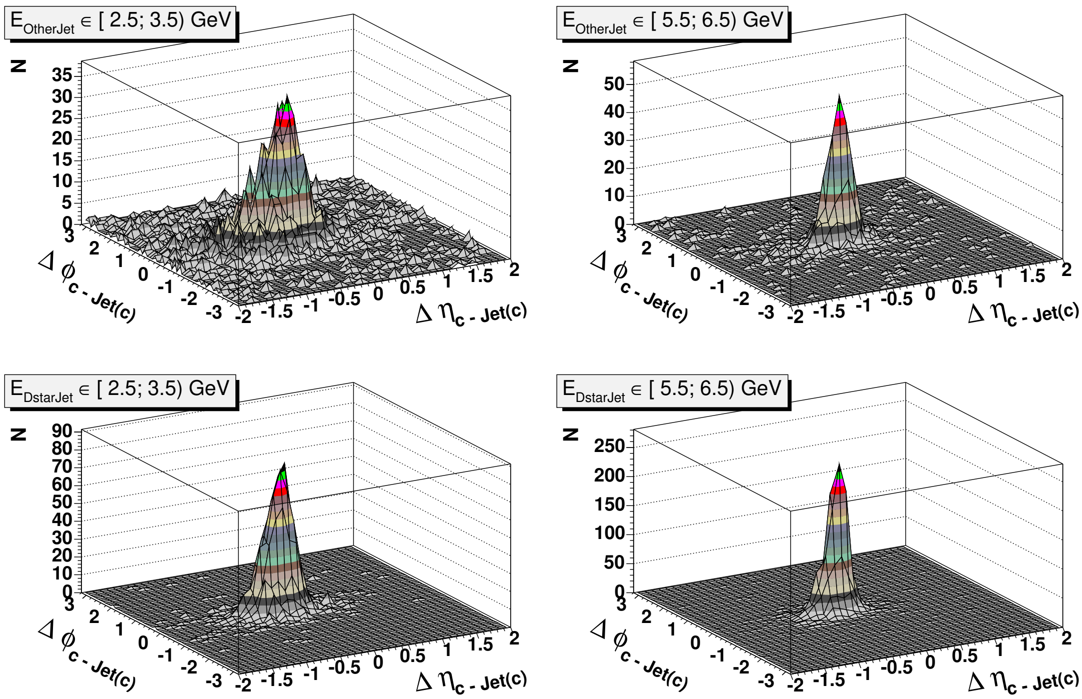

Figure 4: The correlation between the directions of the D^*Jet and the corresponding charm quark (the generated c or $\bar{c}$ is chosen according to the charge of the D^*-meson) is shown in the lower row; idem for the $Other$Jet and the corresponding charm quark (the upper row).

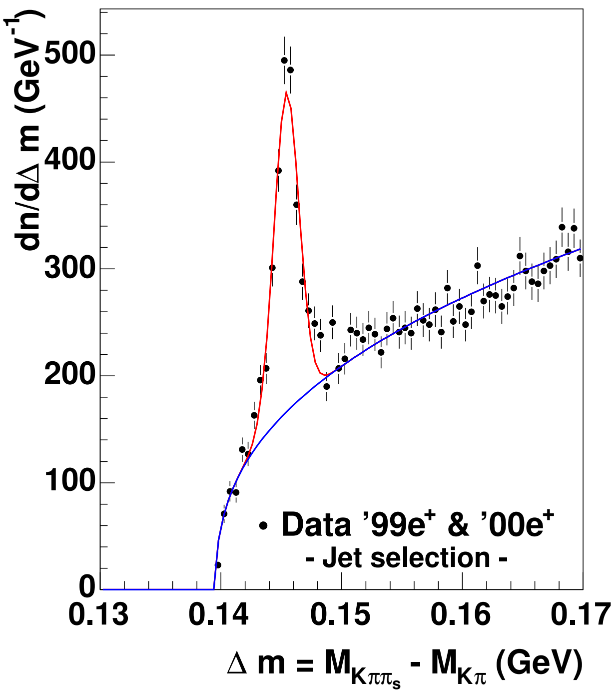

Figure 5: The distribution of the mass difference $\Delta m = m(K^{\mp}\pi^{\pm}\pi_{\mathrm{s}}^{\pm}) - m(K^{\mp}\pi^{\pm})$

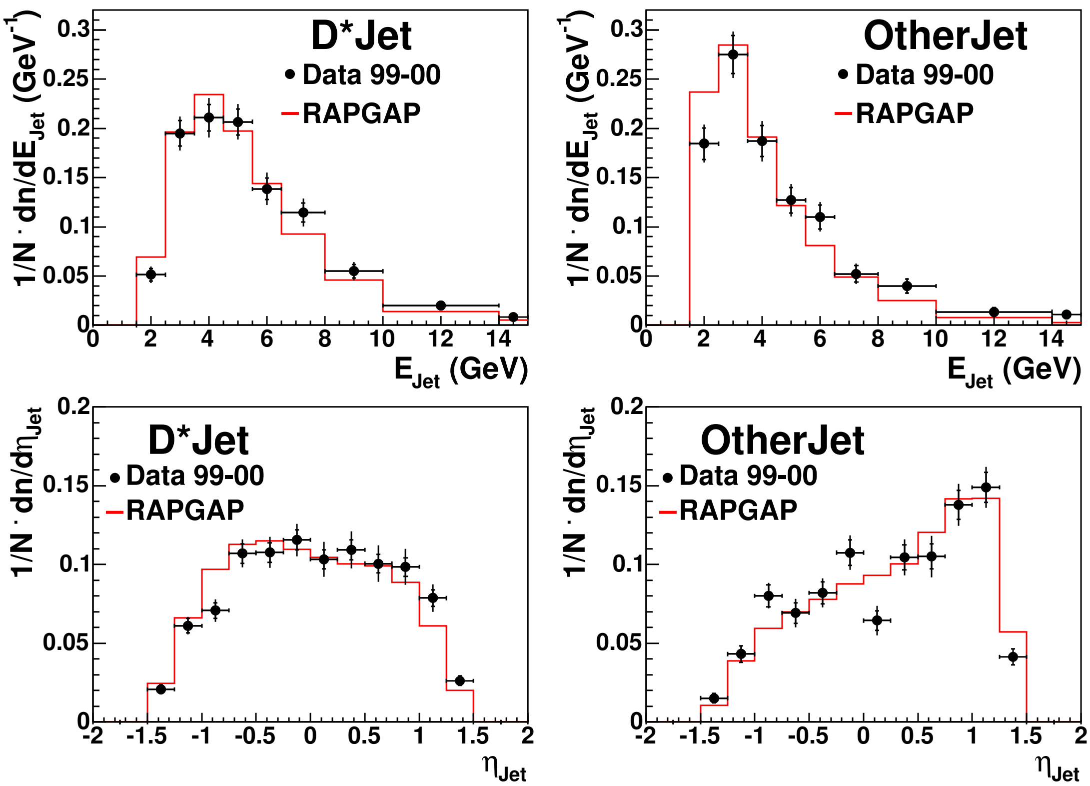

Figure 6: The energy and pseudorapidity distributions compared to the QCD model predictions for the D^*Jet, left column, and the $Other$Jet, right column.

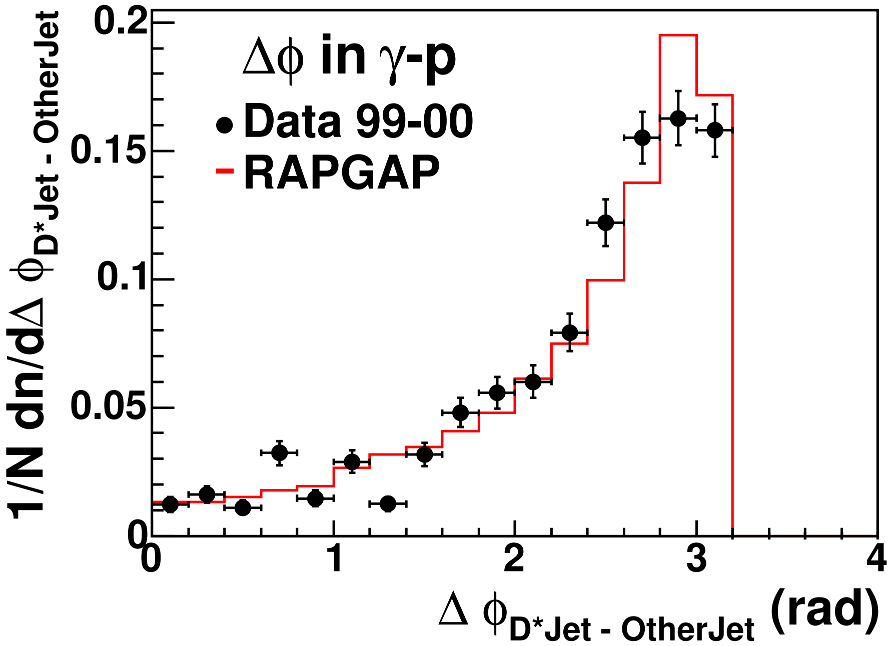

Figure 7: $\Delta\phi$ between the D^*Jet and the $Other$Jet in the γp- frame.

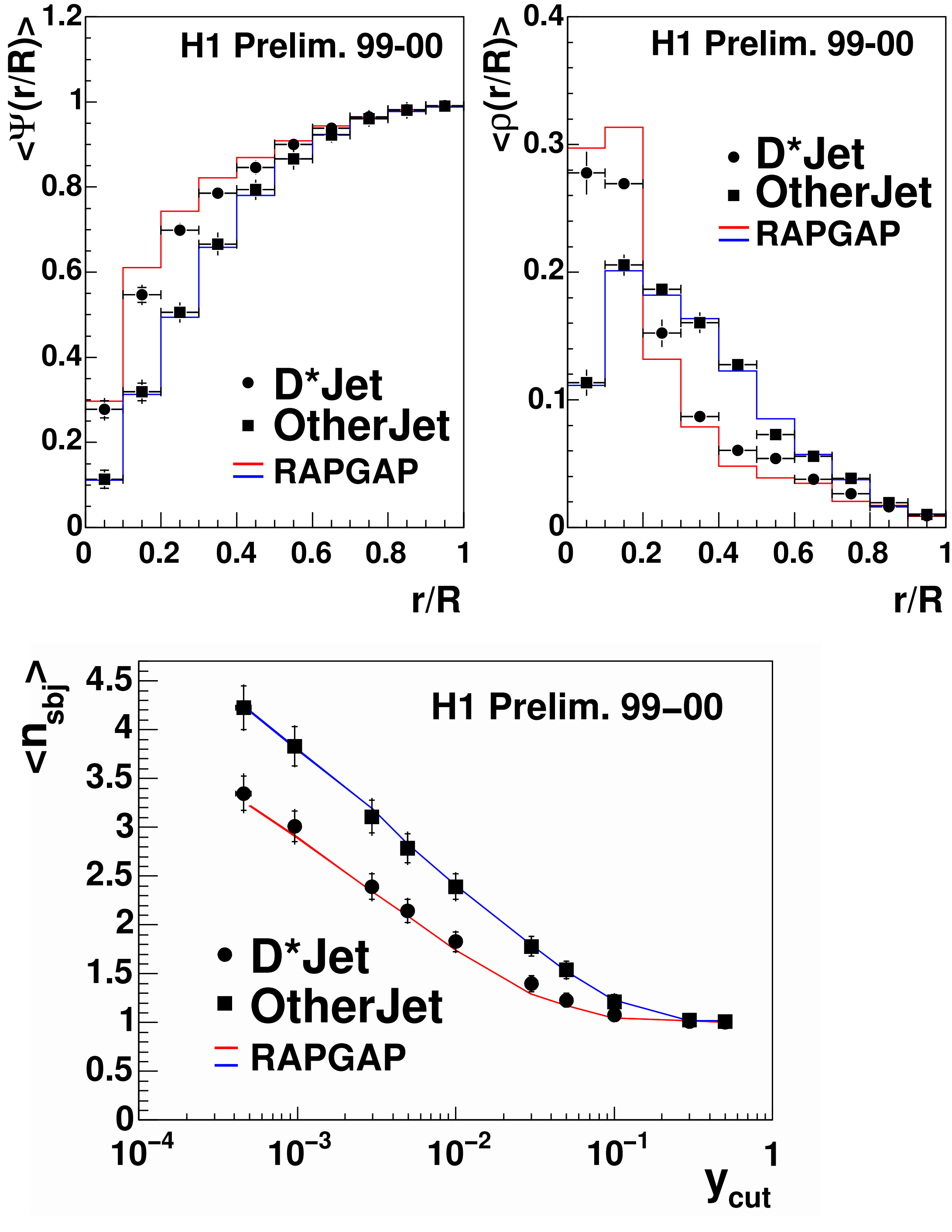

Figure 8: The measured jet shape observables for the D^*Jet (full circles), and for the $Other$Jet (full squares). The solid lines show the predictions from the QCD model.

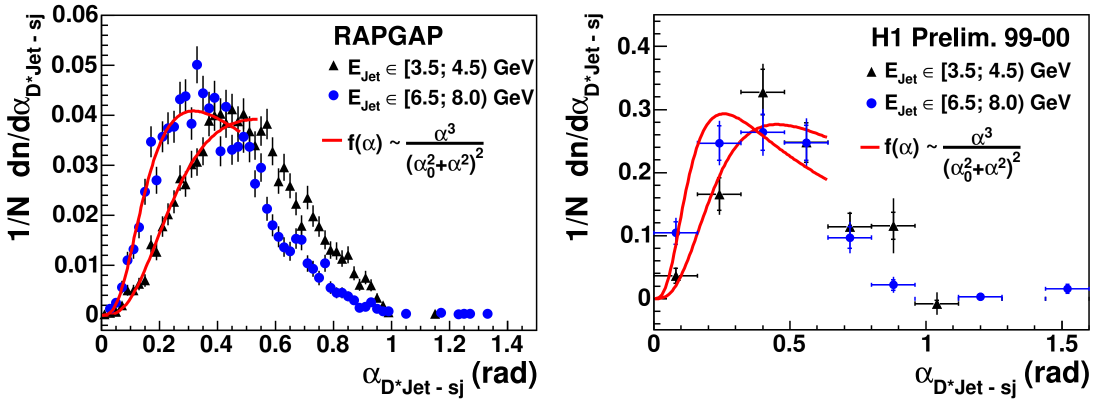

Figure 9: The distribution of the angle α between the "gluon" subjet and the D^*Jet for two bins in jet energy for data (right) and the QCD model RAPGAP 2.8 after full detector simulation and reconstruction (left). The solid lines indicate the results of the fit using the function $f(\alpha) \sim \alpha^3/(\alpha_0^2 + \alpha^2)^2$ predicted by the QCD theory.

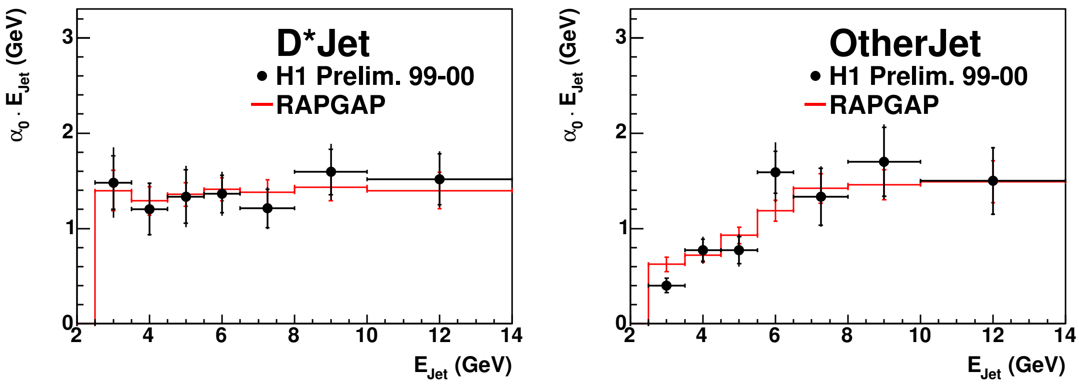

Figure 10: $\alpha_0 \cdot < E_{\rm jet} >$ as a function of $< E_{\rm jet} >$ for the D^*Jet and the $Other$Jet compared to QCD model predictions of RAPGAP 2.8/JETSET 7.4.

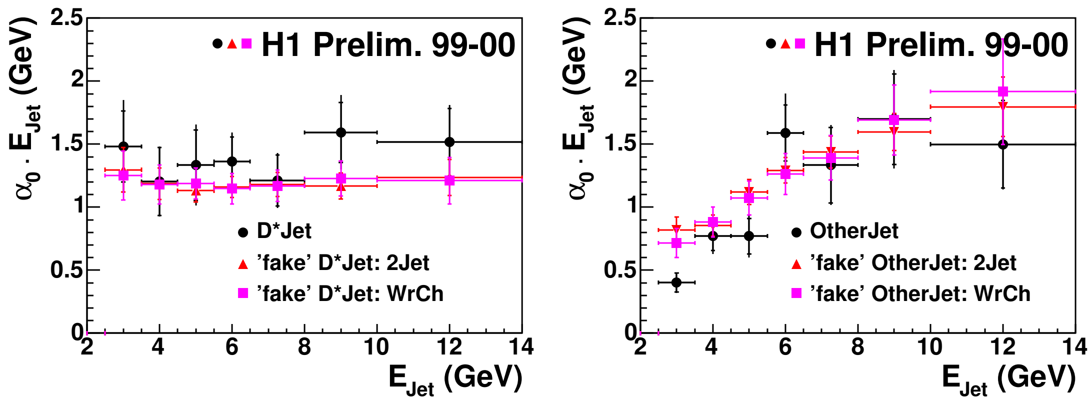

Figure 11: $\alpha_0 \cdot < E_{\rm jet} >$ as a function of $< E_{\rm jet} >$ for the D^*Jet and the $Other$Jet (same data as above) compared to "fake" D^*Jet in wrong charge (WrCh) combinations and in flavor-unbiased selected (u, d, s, c) dijets (see also text).